JACS
JOURNAL OF THE AMERICAN CHEMICAL SOCIETY
Article
pubs.acs.org/JACS

Realizing Ferromagnetic Coupling in Diluted Magnetic Semiconductor Quantum Dots

Wensheng Yan,† Qinghua Liu,† Chao Wang, Xiaoyu Yang, Tao Yao, Jingfu He, Zhihu Sun,* Zhiyun Pan, Fengchun Hu, Ziyu Wu,* Zhi Xie, and Shiqiang Wei*

National Synchrotron Radiation Laboratory, University of Science and Technology of China, Hefei, Anhui 230029, China

Supporting Information

ABSTRACT: Manipulating the ferromagnetic interactions in diluted magnetic semiconductor quantum dots (DMSQDs) is a central theme to the development of next-generation spin-based information technologies, but this remains a great challenge because of the intrinsic antiferromagnetic coupling between impurity ions therein. Here, we propose an effective approach capable of activating ferromagnetic exchange in ZnO-based DMSQDs, by virtue of a core/shell structure that engineers the energy level of the magnetic impurity 3d levels relative to the band edge. This idea has been successfully applied to $Zn_{0.96}Co_{0.04}O$ DMSQDs covered by a shell of ZnS or Ag_2S. First-principles calculations further indicate that covering a ZnS shell around the Co-doped ZnO core drives a transition of antiferromagnetic-to-ferromagnetic interaction, which occurs within an effective depth of 1.2 nm underneath the surface in the core. This design opens up new possibility for effective manipulation of exchange interactions in doped oxide nanostructures for future spintronics applications.

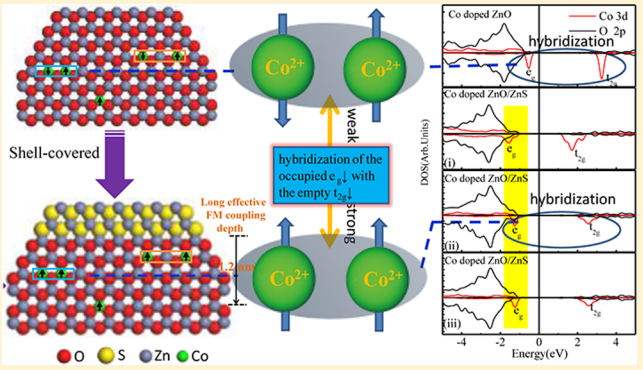

INTRODUCTION

Diluted magnetic semiconductor quantum dots (DMSQDs) of several nanometers present a promising material for the future quantum computer and many other spin-based information technologies, due to their long spin coherence times and the capability of manipulating the current spin polarization under a weak external field.[1−9] Because the magnetic exchange interactions (between carriers and magnetic ions or between magnetic ions and magnetic ions) determine to a large extent the optical, electronic, and magnetic properties of the DMSQDs, how to manipulate the exchange interactions therein has become a key issue.[9,10] Co-doped ZnO nanostructures have been most intensely studied as a prototypical model system to clarify the origin of magnetic exchange interactions.[11−14] By using strategies of codoping or annealing treatment to induce localized or iterant carriers, ferromagnetic ordering has been stabilized in a lot of Co-doped ZnO nanocrystals synthesized by colloidal chemistry, such as nanorods,[15,16] nanowires,[17,18] and nanoparticles (diameter >20 nm),[11,19,20] all of which have sizes beyond the limit of quantum confinement effect. However, in the size region where strong quantum confinement occurs, it exerts two adverse impacts on the magnetic couplings between Co ions. First, the quantum confinement upshifts the energy levels of the donor defects while the Co 3d states are pinned at the same position as in bulk,[21,22] which reduces the interactions between the defect-bound electrons and magnetic dopants. Second, due to the quantum confinement, the carriers (localized or delocalized) possess partial p-character and they are mixed with the Bloch functions of the 4s conduction band at finite k vector,[23,24] further suppressing the ferromagnetic couplings between Co^{2+}. Therefore, introducing extra charge carriers to realize ferromagnetic interactions in DMSQDs is not an ideal pathway. In fact, the routinely used methods for DMSs of relatively large size to tune magnetic couplings, like codoping or annealing under different atmospheres, could hardly be used for DMSQDs, because of the self-purification or size growth of the QDs in the heating process.[25] To realize ferromagnetic coupling between magnetic ions in Co-doped ZnO quantum dots still remains rather challenging.

Recently, great efforts have been attempted and progress has been made in activating the ferromagnetism of quantum-confined DMS nanostructures. One example is the work by Beaulac and co-workers,[5] who used photoexcitation to generate excitonic magnetic polarons (EMP) and realized ferromagnetic Mn−Mn couplings at the nanosecond time scale in Mn-doped CdSe quantum dots. Ochsenbein et al.[3] observed a large room-temperature ferromagnetic responses in vacuum for colloidal Mn-doped ZnO quantum dots, using an anaerobic ultraviolet (UV) photoexcitation to inject electrons into the conduction band. However, the ferromagnetic coupling between ions in these DMS quantum dots is not intrinsic but could only be activated under some extreme external conditions. According to the band coupling model,[10,26] there is a competition between

Received: November 27, 2013
Published: December 31, 2013

   dx.doi.org/10.1021/ja411900w | J. Am. Chem. Soc. 2014, 136, 1150−1155

the ferromagnetic and antiferromagnetic $Co^{2+}-Co^{2+}$ couplings in Co-doped II–IV DMS: ferromagnetic coupling arises from the hybridization of the occupied $e_g\downarrow$ states with the empty $t_{2g}\downarrow$ states, while antiferromagnetic exchange originates from the hybridization of the occupied $t_{2g}\uparrow$ states with the empty $t_{2g}\downarrow$ states. Due to the localized feature of the $e_g\downarrow$ states, the dominant $Co^{2+}-Co^{2+}$ exchange interactions are antiferromagnetic. Therefore, strengthening the ferromagnetic interactions in Co-doped II–IV DMSQD calls for effective approaches to enhance the hybridization of the occupied $e_g\downarrow$ states with the empty $t_{2g}\downarrow$ states. Methods that could change the relative positions of the Co 3d states within the band gap and delocalize the $e_g\downarrow$ state are worth pursuing. When the small size and large specific surface area of QDs are considered, the electronic structures of Co ions in DMSQDs are more prone to surface modifications. Then it could be anticipated that the $Co^{2+}-Co^{2+}$ exchange interactions in DMSQDs cores could be effectively tuned by covering shell materials with different electronic properties (Figure 1).

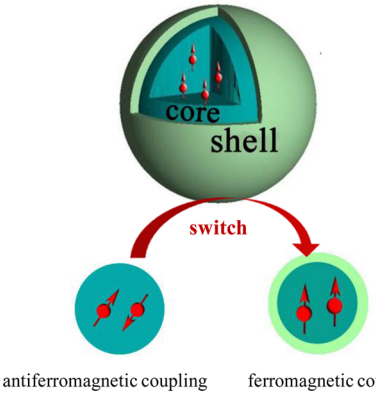

Figure 1. Diagrammatic representation of the ferromagnetic manipulating principle in DMS quantum dots by use of core/shell nanostructure.

In this paper, we propose the idea of using core/shell structures as a platform to tune magnetic interactions in DMS nanostructures. Core/shell structures with different shell materials can bring on tremendous changes in the band gap and the electronic structure of magnetic impurities, which could help to create unprecedented opportunities to tailor the magnetic exchange interactions of DMSQDs. Experimentally, by growth of a shell of ZnS or Ag_2S around the Co-doped ZnO QDs cores in an epitaxial-like manner, we synthesized Co-doped ZnO/ZnS (type II core/shell) and Co-doped ZnO/Ag_2S (inverted core/shell) core/shell structures, which are demonstrated to be able to turn the magnetic couplings within the Co-doped ZnO QDs from antiferromagnetic into ferromagnetic. First-principles calculations exhibit shell-induced changes in the Co-doped ZnO band structure and in the Co 3d electronic states, revealing the microscopic mechanism governing this magnetic change. This design opens up possibilities for effective tuning of the magnetism of doped oxide semiconductor nanostructures for spintronics applications.

EXPERIMENTAL SECTION

Synthesis of Co-Doped ZnO/ZnS Core/Shell Quantum Dots. Co-doped ZnO/ZnS core/shell quantum dots were prepared according to a two-step synthetic method. Generally, the Co-doped ZnO quantum dots were prepared in the first step and ZnS shells were created later via a surface-converting strategy. To prepare the Co-doped ZnO quantum dots, zinc acetate (3.6 mmol) and cobalt acetate (0.36 mmol) were added into a flask with 50 mL of ethanol. The resulting mixture was heated to the boiling point under vigorous stirring. Then 4.6 mL of freshly prepared sodium hydroxide ethanolic solution (1.5 M) was quickly added. The reaction ran for 35 min and the solution was then cooled to room temperature. Excess ethyl acetate was dropped in until precipitation occurred. The precipitate was centrifuged, washed with ethyl acetate several times, and resuspended in ethanol. A clear blue suspension of Co-doped ZnO quantum dots was obtained. Thioacetamide (TAA) was used in the second step as the source of S^{2-} ions. The suspension of quantum dots was mixed with 2 mL of TAA alcoholic solution (0.213 M) and bath-sonicated for 10 min. Then the mixture was heated to the boiling point under stirring. Heating was stopped after 1 h, and stirring lasted for another 8 h. The S^{2-} released by TAA converted the nanoparticle's surface layer from zinc oxide into zinc sulfide. The Co-doped ZnO/ZnS core/shell quantum dots was precipitated by use of ethyl acetate. The precipitate were centrifuged, washed with ethyl acetate, and heated in 10 mL of dodecylamine at about 50 °C under ultrasonic vibration to wipe off the potential residual-free ions. The final product was further centrifuged and suspended in toluene.

The Co-doped ZnO/ZnS core/shell quantum dots can be further converted into Co-doped ZnO/Ag_2S core/shell quantum dots because of the large difference in solubility [the solubility product constant (K_{sp}) of ZnS is 2.93×10^{-25}, while K_{sp} of Ag_2S is 6.69×10^{-50}). Twenty milliliters of $AgNO_3$ alcoholic solution was added dropwise into the suspension of Co-doped ZnO/ZnS core/shell quantum dots under ultrasonic vibration. The product was then centrifuged, washed, treated with dodecylamine, and suspended in toluene as described before.

Structure and Property Characterization. Dopant concentrations were determined by inductively coupled plasma atomic emission spectrometry (ICP-AES, Jarrel Ash model 955). Transmission electron microscopy (TEM) experiments were performed with a JEM-2100 microscope (200 kV). To avoid the influence of toluene's UV absorption, the synthesis of samples for UV–vis absorption experiments was slightly different from the method described previously. Instead of treatment with dodecylamine and suspension in toluene, the quantum dots were directly suspended in ethanol. X-ray diffraction (XRD) patterns were measured with a TTR-III X-ray diffractometer. The Co $L_{2,3}$-edge X-ray absorption near-edge (XANES) spectra were measured at beamline U19 of the National Synchrotron Radiation Laboratory (NSRL) in the total electron yield (TEY) mode by collecting sample drain current under a vacuum better than 5×10^{-8} Pa. The beam from a bending magnet was monochromatized with a varied line-spacing plane grating and refocused by a toroidal mirror. An energy range from 100 to 1000 eV was covered with an energy resolution of about 0.2 eV. The Co K-edge XAFS spectra were measured at the U7C beamline of NSRL, the 1W1B beamline of the Beijing Synchrotron Radiation Facility (BSRF), China, and the BL14W1 beamline of the Shanghai Synchrotron Radiation Facility (SSRF), China. The electron-beam energy of NSRL was 0.8 GeV and the stored current was between 250 and 300 mA. The storage ring of BSRF was operated at 2.5 GeV with a maximum current of 250 mA, and the storage ring of SSRF worked at 3.5 GeV with a maximum current of 210 mA. The O K-edge X-ray absorption fine structure (XAFS) spectra were measured at the U19 beamline of NSRL and BL08U beamline of SSRF in the TEY mode. Magnetic data were collected with a Quantum Design MPMS-5 superconducting quantum interference device (SQUID) magnetometer on sealed air-free colloidal suspensions in toluene. The excitation wavelength was 325 nm. Electronic paramagnetic resonance (EPR) measurements were performed in a JSE-FA200 EPR spectrometer at X-band (~9 GHz) with a resolution of 2.35 μT at room temperature.

RESULTS AND DISCUSSION

The synthetic strategy for $Zn_{0.96}Co_{0.04}O$/ZnS core/shell quantum dots has two steps as schematically shown in Figure

dx.doi.org/10.1021/ja411900w | J. Am. Chem. Soc. 2014, 136, 1150–1155

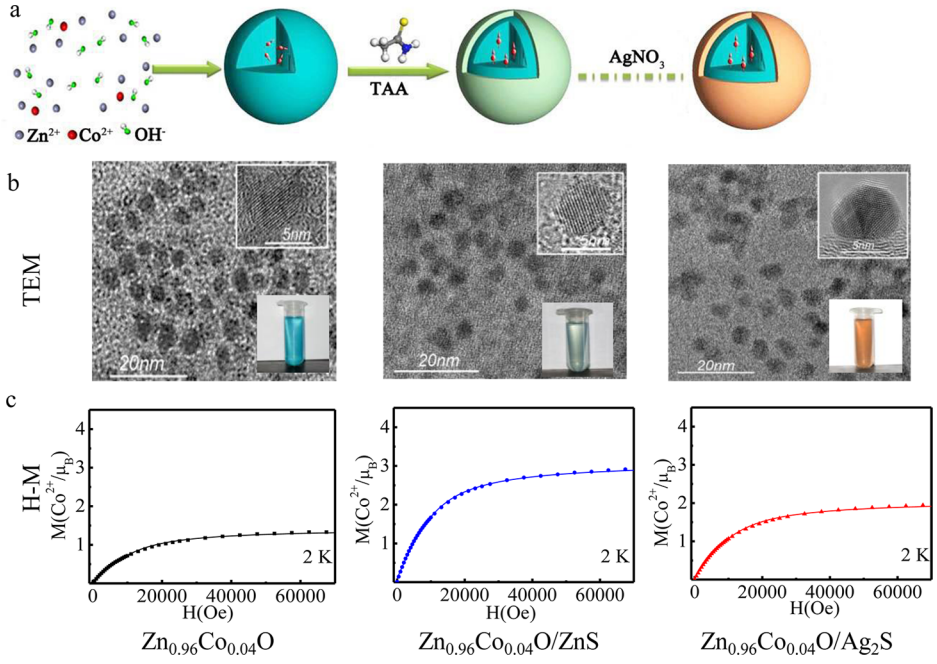

Figure 2. Diagrammatic representation of the synthesis of core/shell quantum dots and characterization of their morphology and magnetic properties. (a) Schematic representation of the quantum dot synthesis. (b) TEM images of representative $Zn_{0.96}Co_{0.04}O$, $Zn_{0.96}Co_{0.04}O/ZnS$, and $Zn_{0.96}Co_{0.04}O/Ag_2S$ quantum dots. (Top insets) High-resolution TEM images of single quantum dots. (Bottom insets) Colors of $Zn_{0.96}Co_{0.04}O$, $Zn_{0.96}Co_{0.04}O/ZnS$, and $Zn_{0.96}Co_{0.04}O/Ag_2S$ suspensions in ethanol. (c) Field dependence of magnetization of $Zn_{0.96}Co_{0.04}O$, $Zn_{0.96}Co_{0.04}O/ZnS$, and $Zn_{0.96}Co_{0.04}O/Ag_2S$ (2 K).

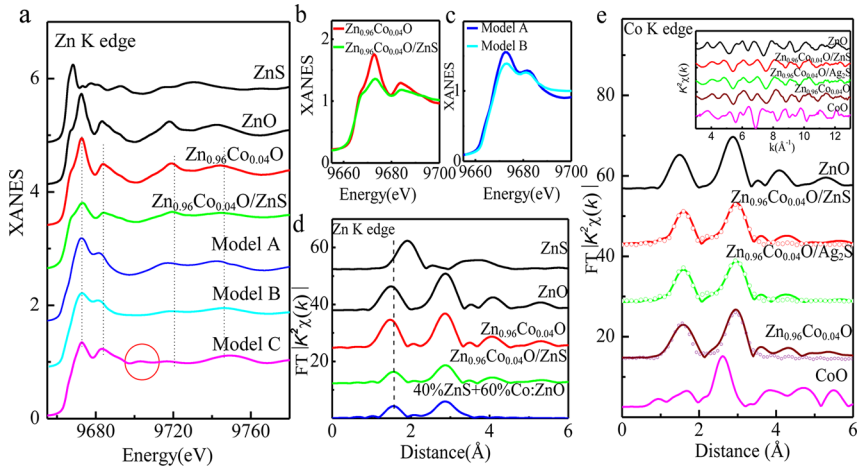

Figure 3. Determination of core/shell structures and occupation sites of magnetic ions. (a) Experimental Zn K-edge XANES spectra of ZnO, ZnS, $Zn_{0.96}Co_{0.04}O$, and $Zn_{0.96}Co_{0.04}O/ZnS$ and calculated spectra for three model structures: Co-doped ZnO (model A), Co-doped ZnO/ZnS (model B), and ZnO+ZnS (model C). (b) Magnified experimental Zn K-edge XANES spectra of $Zn_{0.96}Co_{0.04}O$ and $Zn_{0.96}Co_{0.04}O/ZnS$. (c) Calculated spectra for models A and B. (d) Fourier transform of Zn K-edge EXAFS $k^2\chi(k)$ functions for ZnO, ZnS, $Zn_{0.96}Co_{0.04}O/ZnS$, and $Zn_{0.96}Co_{0.04}O$ (solid lines). (○) Fitting results. (e) Fourier transform of Co K-edge EXAFS $k^2\chi(k)$ functions for ZnO, $Zn_{0.96}Co_{0.04}O/ZnS$, $Zn_{0.96}Co_{0.04}O/Ag_2S$, $Zn_{0.96}Co_{0.04}O$, and CoO. (Inset) $k^2\chi(k)$ functions. (○) Fitting results.

2a. First, the $Zn_{0.96}Co_{0.04}O$ quantum dots were synthesized by a sol−gel-like method as reported in the literature.[16,27] Second, the ZnS shell was grown on the preformed $Zn_{0.96}Co_{0.04}O$ quantum dots by S atoms from TAA that reacted with Zn atoms at the surface of $Zn_{0.96}Co_{0.04}O$.[28] With the growth of a ZnS shell around $Zn_{0.96}Co_{0.04}O$, the color of the suspension gradually changed from blue to light green. In this reaction, Zn atoms in the ZnS shell were pinned at the surface of $Zn_{0.96}Co_{0.04}O$, allowing for confinement of the ZnS shell on the core. After the synthesis of $Zn_{0.96}Co_{0.04}O/ZnS$, an ion replacement reaction was used to produce $Zn_{0.96}Co_{0.04}O/Ag_2S$ by mixing $Zn_{0.96}Co_{0.04}O/ZnS$ with excess $AgNiO_3$ solution. The XRD pattern (Figure S1, Supporting Information) indicates the wurtzite structure in the $Zn_{0.96}Co_{0.04}O$ core, and this structure is maintained after the growth of the ZnS or Ag_2S shell. The crystallinity of the core/shell quantum dots is demonstrated by transmission electron microscopy (TEM) images (including a high-resolution image of a single quantum dot) shown in Figure 2b, which display a roughly spherical shape for the core and core/shell quantum dots with a mean size of 5 nm, smaller than the critical size for quantum confinement in ZnO.[29]

dx.doi.org/10.1021/ja411900w | J. Am. Chem. Soc. 2014, 136, 1150−1155

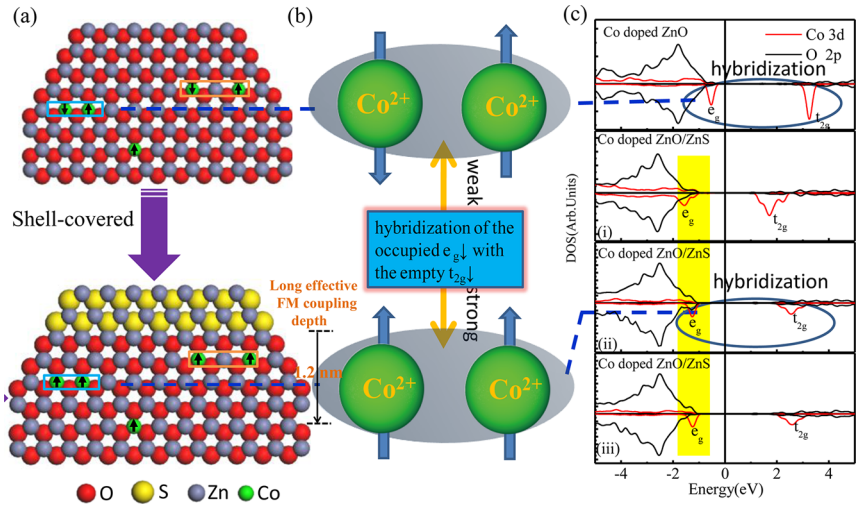

Figure 4. Interactions between core and shell materials in the core/shell quantum dots. (a) Schematic of theoretical model for magnetic interactions between Co ions in different depth layers influenced by the ZnS shell. (b) Schematic for hybridization between Co−Co pairs before and after covering the ZnS shell. (c) Calculated density of states (DOS) for various model structures: Co ions in ZnO without ZnS shell (top panel) and in the second layer (i), third layer (ii), and inner layer (iii) after covering the ZnS shell.

To display the critical role of shell in altering Co^{2+}−Co^{2+} magnetic interactions in the $Zn_{0.96}Co_{0.04}O$ QDs core, we show in Figure 2c the magnetization measurement results for these nanostructures (dilute suspensions of the same colloidal nanocrystals). Solid lines in Figure 2c display the Brillouin function calculated for paramagnetic Co^{2+} ions with spin $S = {}^3/_2$ at 2 K at three different effective concentrations x_{eff}. The 2 K saturation moment for $Zn_{0.96}Co_{0.04}O$ QDs is $1.2\mu_B/Co^{2+}$ (x_{eff}/x = 0.40), significantly smaller than what would be observed if all Co^{2+} ions contributed fully (x_{eff}/x = 1.0, M_{sat} = $3.0\mu_B/Co^{2+}$), in agreement with the results by White and co-workers.[30] This reduction arises from the well-known antiferromagnetic interactions that are active within part of the Co^{2+}−Co^{2+} pairs. After growth of the ZnS shell, the $Zn_{0.96}Co_{0.04}O$ QDs obtained a saturation moment as high as $2.8\mu_B/Co^{2+}$ (x_{eff}/x = 0.93), very close to the theoretical value of $3.0\mu_B/Co^{2+}$ in a tetragonal ligand field. Hence, the Co^{2+}−Co^{2+} magnetic couplings are overwhelmingly turned from antiferromagnetic into ferromagnetic by growth of the ZnS layer. A similar phenomenon is also observed in $Zn_{0.96}Co_{0.04}O/Ag_2S$ synthesized by the same method, but its saturation moment is relatively smaller, $1.8\mu_B/Co^{2+}$ (x_{eff}/x = 0.60) (the difference will be discussed later).

To verify the formation of $Zn_{0.96}Co_{0.04}O$/ZnS core/shell and to determine the ZnS shell thickness, the XAFS technique with element-specific and structure-sensitive features was used to probe their local atomic structures.[31−33] The Zn K-edge XANES spectrum of $Zn_{0.96}Co_{0.04}O$/ZnS exhibits a similar spectral shape to that of $Zn_{0.96}Co_{0.04}O$ quantum dots (Figure 3a), although the white-line peak at ∼9673 eV is significantly reduced in intensity (Figure 3b). We considered several structure models and calculated the Zn K-edge XANES spectra using FEFF8.2 code (see section II in Supporting Information).[34] First, the calculated XANES spectrum for model C (a ZnS−ZnO mixed cluster) presents at 9703 eV a characteristic peak as labeled by a red circle in Figure 3a. The peak position is quite different from that in the spectrum of $Zn_{0.96}Co_{0.04}O$/ZnS quantum dots, suggesting that the two main components of $Zn_{0.96}Co_{0.04}O$/ZnS quantum dots (that is, $Zn_{0.96}Co_{0.04}O$ and ZnS) are not isolated in space. The calculations based on model A (a ZnO cluster composed of 125 atoms, corresponding to a Co-doped ZnO) and model B [a ZnO/ZnS core/shell cluster including 125 atoms (34 O, 34 S and 56 Zn atoms)] could reproduce the main spectral features of the experimental data for $Zn_{0.96}Co_{0.04}O$ and $Zn_{0.96}Co_{0.04}O$/ZnS quantum dots, respectively. Furthermore, the white-line intensity of model B is remarkably reduced as compared to model A (Figure 3c), consistent with the trend of the experimental observations (Figure 3b). These results provide support for the formation of a ZnS layer on the $Zn_{0.96}Co_{0.04}O$ quantum dot surfaces. In other words, $Zn_{0.96}Co_{0.04}O$/ZnS quantum dots with a core/shell structure have been obtained. Analogously, Guglieri and Chaboy[35] also observed reduced white-line peak intensity for ZnO QDs upon thiol capping, and they ascribed this to formation of Zn−S bonds between Zn and S atoms. Furthermore, from the ZnS/ZnO molar ratio (40:60) obtained from quantitative EXAFS data analysis (Figure 3d) and considering the particle size (∼5 nm), a ZnS shell thickness of about 0.55 nm can be estimated (see section III in Supporting Information). Similar phenomena of using a 0−0.8 nm thick CdSe-like shell to effectively change the magnetic couplings in Mn- or Cu-doped ZnSe QDs have also been reported.[2,36] We note that, in $Zn_{0.96}Co_{0.04}O/Ag_2S$, there may exist small Ag_2S clusters (islands) on the ZnO QDs surfaces and only core/shell alike structure is formed, because the lattice structures of Ag_2S and ZnO are significantly different. In addition, detailed analysis of EXAFS spectra in Figure 3e reveals the substitution of Co for Zn sites in all these QDs (see section IV in Supporting Information), and within the detection limit of XAFS, no Co-related secondary phase could be detected upon covering the ZnS or Ag_2S shell on the $Zn_{0.96}Co_{0.04}O$ cores. These results lead us to conclude that the significantly enhanced saturation magnetic moment of $Zn_{0.96}Co_{0.04}O$/ZnS and $Zn_{0.96}Co_{0.04}O/Ag_2S$ QDs indeed arises from modified exchange interactions between substitutional Co ions.

Next, for an in-depth understanding of the origin of the altered Co^{2+}−Co^{2+} magnetic exchange interactions by a ZnS shell covering $Zn_{0.96}Co_{0.04}O$ QDs, we employed Vienna ab initio simulation package (VASP) calculations to investigate the electronic structure changes. Details of the calculations are

dx.doi.org/10.1021/ja411900w | J. Am. Chem. Soc. 2014, 136, 1150−1155

included in Supporting Information (section V). The formation energy calculations suggest that, afterZnS shell covering, the exchange interactions between Co^{2+} ion pairs near the QD surface turn from antiferromagnetic to ferromagnetic, no matter whether they are nearest neighbors or next-nearest neighbors (see the Co^{2+}−Co^{2+} pairs labeled in Figure 4a). Especially, the formation energy for the nearest neighboring Co^{2+}−Co^{2+} pair located at the fourth Zn−O layer underneath the ZnS shell (about 1.2 nm in depth) still keeps at the level of −0.21 eV. Assuming that all the Co ions are homogeneously distributed in Co-doped ZnO/ZnS, we estimated that the interactions between Co ions located within a depth of 1.2 nm underneath the ZnO surface are changed from antiferromagnetic to ferromagnetic. In other words, about 90% of Co atoms contribute to the ferromagnetic ordering, in agreement with the saturation magnetic moment measurement (Figure 2c). Inferred from the obtained density of states (DOS) as shown in Figure 4c, such a change in magnetic interactions is intimately related to modifications of the electronic structures. In Co-doped ZnO, the tetrahedral symmetry around Co atoms splits the Co 3d levels into a doubly degenerate e_g band and a triply degenerate t_{2g} band. The ground state of Co^{2+} is in a high-spin d^7 ($S^{3/2}$) configuration. All the Co^{2+} spin-up 3d levels are covalently delocalized into the valence band (VB) of the ZnO semiconductor host, but the spin-down $e_g\downarrow$ level is remarkably higher in energy than the edge of VB (O 2p) and displays localized character. However, in Co-doped ZnO/ZnS, the band gap of ZnO is considerably narrowed, as also indicated by the electronic absorption spectra (see section VI in Supporting Information). This comes from the O 2p energy position engineering, which has at least two reasons: the interactions between S 3p and O 2p states at the interface of the core/shell as well as the strain due to the lattice mismatch between ZnO and ZnS.[37] As a result, hybridization between O 2p and Co 3d states is enhanced. More importantly, the strong hybridization between Co 3d $e_g\downarrow$ and VB renders delocalized feature to the Co 3d $e_g\downarrow$ state (see panel i in Figure 4c). Meanwhile, the energy difference of $e_g\downarrow$ and $t_{2g}\downarrow$ is reduced from 3.77 to 3.26 eV, which, according to the band coupling model,[10,26] is favorable for the increase of the energy gain ΔE^{FM} and ferromagnetic exchange of the Co^{2+}−Co^{2+} interactions (Figure 4b). This suggests that, under a certain temperature, the Co:ZnO/ZnS nanocrystals exhibit a macroscopically ferromagnetic property. Of note, the energy gain $\Delta E^{FM} \propto 1/[E(t_{2g}\downarrow) - E(e_g\downarrow)]$ of the $t_{2g}\downarrow$−$e_g\downarrow$ hopping is expected to be considerably smaller than that of $t_{2g}\downarrow$−$t_{2g}\uparrow$ hopping, since the $e_g\downarrow$ orbitals are highly localized. Besides, on the basis of DOSs of Co ions at various sites, we find that as the Co ions move apart from the ZnS shell, hybridization between Co 3d $e_g\downarrow$ and O 2p$\downarrow$ is weakened (see the yellow region in Figure 4c), and the energy difference between $e_g\downarrow$ and $t_{2g}\downarrow$ is enlarged. Therefore, in the central part of the quantum dots, the dominant Co^{2+}−Co^{2+} interaction is still antiferromagnetic. Recently, Chen et al.[38] manipulated the saturation magnetic moment and coercivity of the Pt/$Zn_{0.95}Co_{0.05}O$/Pt device by changing the distribution of oxygen vacancy using an external electric field, which provides more evidence for the important role of oxygen vacancies in mediating the ferromagnetic ordering of Co:ZnO materials. By contrast, in our samples, the prominent role of oxygen-vacancy-induced carrier in mediating the ferromagnetic coupling could be ruled out by the electronic paramagnetic resonance (EPR) and O K-edge XANES spectra, both of which indicate that covering the ZnS shell does not cause obvious change of the oxygen vacancy concentration. Moreover, we have measured the photoluminescence (PL) spectra of undoped ZnO and ZnO/ZnS, which also suggest that covering a ZnS shell does not enhance the concentration of oxygen vacancy (see section VII in Supporting Information). In Mn-doped II−VI QDs, recent first-principles calculations also suggest a tunable Mn^{2+}−Mn^{2+} exchange by tailoring the quantum confinement even at fixed carrier concentration.[39]

The $Zn_{0.96}Co_{0.04}O/Ag_2S$ heterostructure (inverted core/shell structure) also evidences the capability of manipulating the exchange interaction between Co^{2+} in $Zn_{0.96}Co_{0.04}O$ quantum dots via core/shell structure. This type of core/shell structure is different from $Zn_{0.96}Co_{0.04}O$/ZnS in that the conduction band of the core is higher in energy than that of the shell (Figure S5b, Supporting Information). In analogy to $Zn_{0.96}Co_{0.04}O$/ZnS, the formation of a Ag_2S shell also increases the saturation moment of $Zn_{0.96}Co_{0.04}O$ quantum dots (Figure 2c). However, compared to $Zn_{0.96}Co_{0.04}O$/ZnS, the saturation magnetic moment of $Zn_{0.96}Co_{0.04}O/Ag_2S$ is noticeably lower. We compare in Figure S8 (Supporting Information) the Co $L_{2,3}$ spectra of $Zn_{0.96}Co_{0.04}O/Ag_2S$ and $Zn_{0.96}Co_{0.04}O$/ZnS. When the shell material is changed from ZnS to Ag_2S, the characteristic peak at about 770 and 784 eV arising from electron transition from Co 2p to Co 3d is increased in intensity, suggesting higher Co 3d electron occupation in $Zn_{0.96}Co_{0.04}O$/ZnS. Therefore, compared with $Zn_{0.96}Co_{0.04}O/Ag_2S$, the hybridization between O 2p and Co 3d states is stronger in $Zn_{0.96}Co_{0.04}O$/ZnS, and the Co^{2+}−Co^{2+} interactions are easier to switch from antiferromagnetic to ferromagnetic, resulting in the much higher saturation magnetic moment of $Zn_{0.96}Co_{0.04}O$/ZnS as observed. The different hybridization strength of O 2p and Co 3d can also be confirmed experimentally by comparison of the Co K-edge XANES spectra of $Zn_{0.96}Co_{0.04}O/Ag_2S$ and $Zn_{0.96}Co_{0.04}O$/ZnS QDs (Figure S9, Supporting Information). In spite of their similar XANES features in the post-edge region, a slight difference occurs at the pre-edge peak A (7709 eV) that is associated with electron transition from Co 1s to Co 3d−O 2p hybridized states.[40] The lower intensity of the pre-edge peak A of $Zn_{0.96}Co_{0.04}O$/ZnS over $Zn_{0.96}Co_{0.04}O/Ag_2S$ indicates less occupied 3d states in $Zn_{0.96}Co_{0.04}O$/ZnS. On the basis of these results, we believe that changing the core/shell band alignment indeed provides an effective route to tailor the magnetic states of DMS quantum dots.

■ CONCLUSION

In conclusion, using the Co-doped ZnO system as an example, we have experimentally demonstrated the feasibility of tuning the interactions between magnetic impurities in transition metal doped oxide semiconductor quantum dots by engineering the energy level of the magnetic impurity 3d levels within the band gap using a core/shell structure. As shown by a detailed study of structural and magnetic properties, this concept is applicable to $Zn_{0.96}Co_{0.04}O$/ZnS and $Zn_{0.96}Co_{0.04}O/Ag_2S$ heterostructures. We expect that this idea can be generalized to tune the magnetic properties of other materials, and it opens up new possibilities for effective manipulation of exchange interactions in doped oxide nanostructures for future spintronics applications.

dx.doi.org/10.1021/ja411900w | J. Am. Chem. Soc. 2014, 136, 1150−1155

■ ASSOCIATED CONTENT

Supporting Information

Additional text, nine figures, and three tables showing XRD results, details of XANES calculations, estimation of shell thickness, determination of occupation sites of Co ions, first-principles modeling and calculation details, influence of ZnS shell on band structure of $Zn_{0.96}Co_{0.04}O$ quantum dots, determination of oxygen vacancy, and XAS and XANES spectra. This material is available free of charge via the Internet at http://pubs.acs.org.

■ AUTHOR INFORMATION

Corresponding Authors

zhsun@ustc.edu.cn
wuzy@ustc.edu.cn
sqwei@ustc.edu.cn

Author Contributions

[†]W.Y. and Q.L. contributed equally to this work.

Notes

The authors declare no competing financial interest.

■ ACKNOWLEDGMENTS

This work was supported by National Natural Science Foundation of China (Grants 11135008, 11079004, U1332131, 11175184, and 11305172), the Foundation for Innovative Research Groups of the National Natural Science Foundation of China (11321503), National Basic Research Program of China (2012CB825800), and New Century Excellent Talents in Chinese University. We are grateful to NSRL, BSRF and SSRF for the valuable beamtime.

■ REFERENCES

(1) Erwin, S. C.; Zu, L.; Haftel, M. I.; Efros, A. L.; Kennedy, T. A.; Norris, D. J. *Nature* **2005**, *436*, 91−94.
(2) Bussian, D. A.; Crooker, S. A.; Yin, M.; Brynda, M.; Efros, A. L.; Klimov, V. I. *Nat. Mater.* **2009**, *8*, 35−40.
(3) Ochsenbein, S. T.; Feng, Y.; Whitaker, K. M.; Badaeva, E.; Liu, W. K.; Li, X. S.; Gamelin, D. R. *Nat. Nanotechnol.* **2009**, *4*, 681−687.
(4) Viswanatha, R.; Pietryga, J.; Klimov, V.; Crooker, S. *Phys. Rev. Lett.* **2011**, *107*, No. 067402.
(5) Gamelin, D. R.; Beaulac, R.; Schneider, L.; Archer, P. I.; Bacher, G. *Science* **2009**, *325*, 973−976.
(6) Chen, O.; Shelby, D. E.; Yang, Y.; Zhuang, J.; Wang, T.; Niu, C.; Omenetto, N.; Cao, Y. C. *Angew. Chem., Int. Ed.* **2010**, *49*, 10132−10135.
(7) Gamelin, D. R.; Ochsenbein, S. T. *Nat. Nanotechnol.* **2011**, *6*, 111−114.
(8) Chang, K.; Chan, K.; Peeters, F. *Phys. Rev. B* **2005**, *71*, No. 155309.
(9) Wolf, S. A.; Awschalom, D. D.; Buhrman, R. A.; Daughton, J. M.; von Molnar, S.; Roukes, M. L.; Chtchelkanova, A. Y.; Treger, D. M. *Science* **2001**, *294*, 1488−1495.
(10) Sato, K.; Kudrnovský, J.; Dederichs, P. H.; Eriksson, O.; Turek, I.; Sanyal, B.; Bouzerar, G.; Katayama-Yoshida, H.; Dinh, V. A.; Fukushima, T.; Kizaki, H.; Zeller, R. *Rev. Mod. Phys.* **2010**, *82*, 1633−1690.
(11) Zhang, Z. H.; Wang, X. F.; Xu, J. B.; Muller, S.; Ronning, C.; Li, Q. *Nat. Nanotechnol.* **2009**, *4*, 523−527.
(12) Gamelin, D. R.; Schwartz, D. A.; Norberg, N. S.; Nguyen, Q. P.; Parker, J. M. *J. Am. Chem. Soc.* **2003**, *125*, 13205−13218.
(13) Ciatto, G.; Di Trolio, A.; Fonda, E.; Alippi, P.; Testa, A.; Bonapasta, A. *Phys. Rev. Lett.* **2011**, *107*, No. 127206.
(14) Larde, R.; Talbot, E.; Pareige, P.; Bieber, H.; Schmerber, G.; Colis, S.; Pierron-Bohnes, V.; Dinia, A. *J. Am. Chem. Soc.* **2011**, *133*, 1451−1458.
(15) Qiu, X. Q.; Li, L. P.; Tang, C. L.; Li, G. S. *J. Am. Chem. Soc.* **2007**, *129*, 11908−11909.
(16) Yao, T.; Yan, W. S.; Sun, Z. H.; Pan, Z. Y.; He, B.; Jiang, Y.; Wei, H.; Nomura, M.; Xie, Y.; Xie, Y. N.; Hu, T. D.; Wei, S. Q. *J. Phys. Chem. C* **2009**, *113*, 3581−3585.
(17) Yuhas, B. D.; Fakra, S.; Marcus, M. A.; Yang, P. D. *Nano Lett.* **2007**, *7*, 905−909.
(18) Liang, W. J.; Yuhas, B. D.; Yang, P. D. *Nano Lett.* **2009**, *9*, 892−896.
(19) Zhang, L.-J.; Wang, J.-Q.; Li, J.; Zhou, J.; Cai, W.-P.; Cheng, J.; Xu, W.; Yin, G.; Wu, X.; Jiang, Z.; Zhang, S.; Wu, Z.-Y. *Chem. Commun.* **2012**, *48*, 91.
(20) Shi, T. F.; Zhu, S. Y.; Sun, Z. H.; Wei, S. Q.; Liu, W. H. *Appl. Phys. Lett.* **2007**, *90*, No. 102108.
(21) Gamelin, D. R.; Norberg, N. S.; Dalpian, G. M.; Chelikowsky, J. R. *Nano Lett.* **2006**, *6*, 2887−2892.
(22) Gamelin, D. R.; Badaeva, E.; Isborn, C. M.; Feng, Y.; Ochsenbein, S. T.; Li, X. S. *J. Phys. Chem. C* **2009**, *113*, 8710−8717.
(23) Merkulov, I. A.; Rodina, A. V. In *Introduction to the Physics of Diluted Magnetic Semiconductors*; Kossut, J., Gaj, J. A., Eds.; Springer Series in Materials Science, Vol. *144*; Springer-Verlag: Berlin, 2010; p 65.
(24) Merkulov, I. A.; Yakovlev, D. R.; Keller, A.; Ossau, W.; Geurts, J.; Waag, A.; Landwehr, G.; Karczewski, G.; Wojtowicz, T.; Kossut, J. *Phys. Rev. Lett.* **1999**, *83*, 1431−1434.
(25) Dalpian, G. M.; Chelikowsky, J. R. *Phys. Rev. Lett.* **2006**, *96*, No. 226802.
(26) Belhadji, B.; Bergqvist, L.; Zeller, R.; Dederichs, P. H.; Sato, K.; Katayama-Yoshida, H. *J. Phys.: Condens. Matter* **2007**, *19*, No. 436227.
(27) Liu, T.; Xu, H. R.; Chin, W. S.; Yong, Z. H.; Wee, A. T. S. *J. Phys. Chem. C* **2008**, *112*, 3489−3495.
(28) Zhu, Y. F.; Fan, A. H.; Shen, W. Z. *J. Phys. Chem. C* **2008**, *112*, 10402−10406.
(29) Gamelin, D. R.; Radovanovic, P. V.; Norberg, N. S.; McNally, K. E. *J. Am. Chem. Soc.* **2002**, *124*, 15192−15193.
(30) Gamelin, D. R.; White, M. A.; Ochsenbein, S. T. *Chem. Mater.* **2008**, *20*, 7107−7116.
(31) Yao, T.; Sun, Z. H.; Li, Y. Y.; Pan, Z. Y.; Wei, H.; Xie, Y.; Nomura, M.; Niwa, Y.; Yan, W. S.; Wu, Z. Y.; Jiang, Y.; Liu, Q. H.; Wei, S. Q. *J. Am. Chem. Soc.* **2010**, *132*, 7696−7701.
(32) Yao, T.; Zhang, X. D.; Sun, Z. H.; Liu, S. J.; Huang, Y. Y.; Xie, Y.; Wu, C. Z.; Yuan, X.; Zhang, W. Q.; Wu, Z. Y.; Pan, G. Q.; Hu, F. C.; Wu, L. H.; Liu, Q. H.; Wei, S. Q. *Phys. Rev. Lett.* **2010**, *105*, No. 226405.
(33) Sun, Z. H.; Yan, W. S.; Yao, T.; Liu, Q. H.; Xie, Y.; Wei, S. Q. *Dalton Trans.* **2013**, *42*, 13779−13801.
(34) Ankudinov, A. L.; Ravel, B.; Rehr, J. J.; Conradson, S. D. *Phys. Rev. B* **1998**, *58*, 7565−7576.
(35) Guglieri, C.; Chaboy, J. *J. Phys. Chem. C* **2010**, *114*, 19629−19634.
(36) Xia, Y. N.; Cobley, C. M.; Chen, J. Y.; Cho, E. C.; Wang, L. V. *Chem. Soc. Rev.* **2011**, *40*, 44−56.
(37) Schrier, J.; Demchenko, D. O.; Wang, L. W.; Alivisatos, A. P. *Nano Lett.* **2007**, *7*, 2377−2382.
(38) Chen, G.; Song, C.; Chen, C.; Gao, S.; Zeng, F.; Pan, F. *Adv. Mater.* **2012**, *24*, 3515−3520.
(39) Abolfath, R. M.; Petukhov, A. G.; Zutic, I. *Phys. Rev. Lett.* **2008**, *101*, No. 207202.
(40) Yan, W. S.; Jiang, Q. H.; Sun, Z. H.; Yao, T.; Hu, F. C.; Wei, S. Q. *J. Appl. Phys.* **2010**, *108*, No. 013901.